frontiers in Imaging

TYPE Original Research
PUBLISHED 19 February 2026
DOI 10.3389/fimag.2026.1725794

OPEN ACCESS

EDITED BY
Prasunpriya Nayak,
All India Institute of Medical Sciences Jodhpur, India

REVIEWED BY
Amit Chougule,
University of Michigan, United States
Lei Qin,
Shenzhen Nanshan Hospital, China

*CORRESPONDENCE
Mara Rubia Marques
mara_rubia_marques@ufg.br

RECEIVED 15 October 2025
REVISED 15 January 2026
ACCEPTED 27 January 2026
PUBLISHED 19 February 2026

CITATION
Marques MR, Moreira AC, Mantovani IF, Brito PVA, Nascimento ICGS, Fernandes CP and dos Santos FCA (2026) Aluminum impairs cellular ultrastructure and bone microarchitecture in newborn rats. *Front. Imaging* 5:1725794. doi: 10.3389/fimag.2026.1725794

Aluminum impairs cellular ultrastructure and bone microarchitecture in newborn rats

Mara Rubia Marques[1]*, Anderson Camargo Moreira[2], Iara Frangiotti Mantovani[2], Pedro Vale de Azevedo Brito[3], Isabela Cristina Gomes de Souza Nascimento[1], Celso Peres Fernandes[2] and Fernanda Cristina Alcantara dos Santos[4]

[1]Laboratory of Bone Biology, Institute of Biological Sciences, Department of Histology, Embryology and Cell Biology, Federal University of Goiás, Goiânia, Brazil, [2]Laboratory of Porous Media and Thermophysical Properties (LMPT) - Department of Mechanical Engineering, Federal University of Santa Catarina, Florianópolis, Brazil, [3]One Health Excellence Center, Institute of Biological Sciences, Federal University of Goiás, Goiânia, Brazil, [4]Laboratory of Microscopy applied to Reproduction (LaMARe), Institute of Biological Sciences, Department of Histology, Embryology and Cell Biology, Federal University of Goiás, Goiânia, Brazil

Modern lifestyle is strongly marked by the presence of aluminum (Al) in practically all human consumer products. Bone tissue is one of the main sites of Al accumulation, and its toxic effects are well known in individuals subjected to chronic exposure. However, there is still a gap in knowledge regarding the effects of Al on bone formation in the neonatal period. This study evaluated the effect of Al ingestion on rat tibiae during the neonatal period. Wistar rats were divided into control and Al groups. The Al group received AlCl3 (2.02 mg/kg/day) via gavage for fifteen days, then, the right tibiae were used to evaluate osteoblast and osteocyte ultrastructure and bone microarchitecture using transmission electron microscopy and computed X-ray microtomography, respectively. Al promoted swelling and altered mitochondrial crests in osteoblasts. Osteocytes showed accumulation of electron-dense lysosomes and absence of the osmiophilic lamina in the lacunae, showing characteristics similar to osteocytic osteolysis. Cortical Thickness (Ct.Th), Trabecular thickness (Tb.th) and trabecular number (Tb.N) decreased whilst trabecular spacing (Tb.Sp) increased. These results suggest that Al intake during the neonatal period may affect the function of osteoblasts and osteocytes besides compromising bone formation.

KEYWORDS
aluminum, bone, MET, micro-CT, mitochondria, newborn, osteoblast, osteocyte

1 Introduction

Aluminium (Al) is present in most consumer goods, from drinks and food to personal hygiene products and medicines; these are part of the basic needs for human life, such as feeding, drinking and health care (Lindblad, 2004; Hartung et al., 2025; Yokel, 2020). Yet, numerous studies have shown its toxic effects on different organs, such as brain, kidney, gut, liver, and reproductive and muscleskeleton systems (Yokel, 2020; Hewitt et al., 1990; Hadrup et al., 2024). Its toxicity was firstly described on hemodialysis patients in the 80′s,

correlating Al deposition with osteomalacia and osteoporosis (Cournot-Witmer et al., 1982; Malluche and Faugere, 1988; Klein, 2019). According to Exley (2016) we are living the Aluminum age, and most humans are experiencing chronic intoxication by Al. Young children may ingest more Al than adults and, in some countries, the ingestion is higher than the tolerable Al intake established by governments and organizations (Yokel, 2025). The widespread presence of Al in medicines, parenteral nutrition, and infant formulas is a cause for concern, particularly in the early stages of life. In early 90/s, studies showed that plasma aluminum levels in preterm infants (14.6 μg/L) were higher compared to full-term infants (7.8 μg/L), and it could be related to premature infant formula and/or limited renal capacity of preterm infants to excrete aluminum (Bougle et al., 1991). There is little evidence regarding the effects of Al on bone development during the neonatal period. We have shown previously that Al intake during the neonatal phase induces bone changes similar to osteoporosis, probably through the involvement of osteoblasts (Marques et al., 2022). The present study evaluated the effects of Al intake during the neonatal period on osteoblasts and osteocytes ultrastructure and used X-ray microtomography (micro-CT) reconstruction to correlate bone microarchitecture to the function of osteoblasts and osteocytes.

2 Material and methods

2.1 Animals

Wistar rats (*Rattus norvegicus*) from the UFG Central Animal Facility were used. The animals were kept in the vivarium of the Institute of Biological Sciences of the Federal University of Goiás (UFG), Goiânia. They were housed in polyethylene boxes containing a wood shaving substrate, which was changed every two days. A 12-h light-dark cycle (12 h light/12 h dark) and an average temperature of 23°C were maintained. Filtered water and food (Labina, Purina®) were provided *ad libitum*. The procedures followed the guidelines provided in the guide for care and procedures for laboratory animals and were approved by the institution's Animal Use Ethics Committee (CEUA/UFG protocol no. 100/19).

2.2 Experimental design

Twelve animals were divided into control (C, $n = 6$) and aluminum (AL, $n = 6$) groups. From the 1st to the 15th day after birth, the animals in the control group received, via gavage, 0.9% saline solution and the AL group received an AlCl3 solution [10 mg/kg/day in 0.9% saline solution − 2.02 mg Al/kg/day − 1/35 LD50; adapted from da Silva Lima et al. (2020)] (AlCl3 – Fluka, purity ≥ 99%, LD50: 3,450 mg/kg). After treatment, the animals were euthanized (16th day) by cervical dislocation, and the left and right tibias were harvested for transmission electronic microscopy and micro-CT analyses.

2.3 Transmission electronic microscopy

The left tibia of three animals/group were removed and 1 mm^2 fragments from the subchondral bone were used for the analysis. The samples were fixed in 2.5% glutaraldehyde and 0.2% picric acid in 0.1 M sodium cacodylate buffer, pH 7.2, at 4°C for 48 h, demineralized in a 5% EDTA solution, pH 7.2, at 4°C for 30 days and post-fixed in a 1% osmium tetroxide solution in cacodylate buffer for 18 h at room temperature. The samples were embedded in epoxy resin and ultrathin sections (70 nm) were obtained with an ultramicrotome (Leica EM UC7), positioned on copper grids, and contrasted in a 2% uranyl acetate, and 0.2 lead citrate solutions. The grids were examined with a JEM-2100 transmission electron microscope (Jeol, Akishima, Japan) in the Multi-user High-Resolution Microscopy Laboratory of the Federal University of Goiás (LabMic/UFG, Institute of Physics). Cuboidal cells along the bone matrix surface were considered osteoblasts, whereas cells with cytoplasmic processes that were fully embedded within the bone matrix were considered osteocytes.

2.3.1 RER/Cytoplasm ratio

To determine if Al ingestion affected rough endoplasmic reticulum (RER), we measured the proportional volume ratio RER cistern/Cytoplasm in five osteoblasts of the Control group and eight osteoblasts of the Al group. Only sections of osteoblasts with visible nucleus and plasmatic membrane were analyzed.

2.4 Micro-CT analysis

One specimen from each group was randomly taken, harvested and analyzed with micro-CT as a complementary technique. The specimens were imaged using an XRM Versa-500 (Xradia/Zeiss) micro-CT scanner. The settings used were 50 kV, 4 W, 4.5 s per projection, and no beam hardening filter. The images were filtered using denoising tools and binarized with Avizo. Characterization was then carried out using the ImageJ-BoneJ plugin (Dougherty and Kunzelmann, 2007). Cortical region was imaged with a resolution of 4.5 μm/voxel while the trabecular region was imaged at a resolution of 2 μm/voxel.

The 3D image analysis was performed to determine the following bone parameters: volume/tissue (BV/TV%), cortical thickness (Ct.Th), cortical porosity (Co.Po), cortical number of pores (Ct.np), trabecular thickness (Tb.Th), trabecular spacing (Tb.Sp), and trabecular number (Tb.N). Tb.N represents the density of the bone network (or the number of trabeculae per unit of length) and was determined using the relationship: (BV/TV)/Tb.Th μm^{-1}. These parameters were determined using Dougherty and Kunzelmann (2007) and Chen et al. (2024) BoneJ plugin. This plugin calculates the spaces as the diameter of the largest sphere that fits within a three-dimensional object. In this analysis, the objects of interest were the cortical bone, the trabeculae, and the intertrabecular space.

2.5 Statistical analysis

Quantitative data were analyzed statistically using the "car" package in the R environment (version 4.3.0; R core Team 2018). Data normality was assessed using the Shapiro-Wilk test, and homoscedasticity was evaluated with the Levene's test. Differences between group means were tested using the Student's *t*-test. The level of significance was set at 5% ($p \leq 0.05$). Results are expressed as mean ± standard deviation (SD).

3 Results

3.1 Ultrastructure of osteoblasts and osteocytes

Osteoblasts from the control and Al groups showed similar characteristics as cell morphology, plasmatic membrane integrity and nuclear appearance (Figures 1A, B). In the control group, osteoblasts and osteocytes showed normal mitochondria with intact internal and external membrane (Figures 1C, E, G); however, in the Al group there were distortions in the mitochondrial cristae or disrupted mitochondria (Figures 1D, F, H). The osmiophilic layer at the edge of the lacunae was more frequent in the control group (Figure 1E) and absent in the most lacunae of the Al group (Figure 1F). There was no statistically significant difference in the RER/cytoplasm ratio of osteoblasts between the groups (Figure 1I). The osteocytes of the Al group showed retraction (Figures 1F, H) and higher occurrence of electron-dense lysosomes scattered throughout the cytoplasm (Figure 1H) as observed in osteoblasts (Figures 1B, D).

3.2 Trabecular and cortical bone microarchitecture

The crucial step for achieving a representative trabecular bone analysis in small specimens, such as rats' tibias, is the precise delineation of the volume of interest (VOI). Figure 2a shows a 2D micro-CT slice of the proximal region, where different features are evident across parts (colored squares) of the same anatomical region. Aiming for more representativeness, the largest cylinder inscribed in the subchondral bone (Figure 2b) was chosen as pre-VOI for analysis (2 mm *d* x 2 mm *h*). For the cortical bone, a 2 mm long VOI was taken from the middle of the diaphysis, as can be seen in the digitally opened tibia of Figure 2c.

BV/TV was determined for each slice along the pre-VOI of the trabecular bone (Figure 2b). Figure 3 shows evidence of a distinct variation in the trabecular bone volume, extending from the subchondral region to the center of the tibia. In addition, the curve corresponding to 2D slices from the analyzed VOI were also included. The slice chosen as initial (0 mm) is the first one immediately distal to the epiphyseal cartilage valley. For comparative purposes, the average value was determined across the depth interval of 0 mm to 1.2 mm (VOI) for both groups. Average BV/TV was 24% and 13.7% for Control and Aluminum groups, respectively.

The measurement results of Tb.Th and Tb.Sp can be observed in Figure 4. The scale bar within the figure employs a color gradient to illustrate the range of sizes. It brings the sizes of the biggest and the median trabeculae diameters and the biggest and the median spaces among the trabecular bone according to its colors. For both the Control (Figure 4a) and Al (Figure 4c) groups, the 3D colormaps of the trabecular formation are displayed (Tb.Th), with the first and last corresponding 2D slices positioned alongside them. The same can be found for the space among trabeculae (Tb.Sp) for Control (Figure 4b) and Al (Figure 4d) groups. Table 1 presents the average values for Tb.Th and Tb.Sp, along with the other calculated parameters.

Prior to analyzing cortical bone thickness (Ct.Th), cortical porosity (Co.Po) and the number of pores (Ct.np), the image was pre-processed to eliminate any internal trabecular formation, as indicated by the red arrows in Figures 5a, e. Additionally, the segmented image was processed to eliminate pores before determining Ct.Th (Figures 5b, f). Pores were eliminated (Figures 5c, g) and quantified (Figures 5d, h). The pre- and post-processing procedure of the cortical VOI image was accomplished with Top-Hat filter, arithmetic operations and Analyze Particles tools from ImageJ. The colormap of thicknesses of the cortical bones from Control and Al groups can be found in Figure 6. Even though the cortical bone was thicker in the control group (Figures 6a, b) both control and Al groups had their maximal thickness in the anterior margin of the tibia (whitish color).

4 Discussion

This study showed that AlCl3 feeding during the neonatal period promoted ultrastructural changes in osteoblasts and osteocytes, besides disrupting the trabecular microarchitecture in the tibia of newborn rats. General aspects, such as cell morphology, plasmatic membrane integrity and nucleus appearance were similar in the Control and Al groups. Osteoblasts RER/cytoplasm ratio did not change, suggesting that these cells were active in the Al group and the protein synthesis was supposedly unaffected. On the other hand, there were important mitochondrial changes, such as swelling, a foamy appearance and disruption of the cristae, evidencing that Al caused significant damage to the organelle which could directly affect the quality and quantity of matrix secretion. Also, there were more lysosomes with electron dense content in the osteoblasts and osteocytes of the Al group. Previous studies demonstrated a similar aspect in the female reproductive system (Marwa et al., 2017) and the gastrointestinal tract (Florent et al., 1991), suggesting that lysosomes could be involved in Al elimination. An alternative hypothesis to the number of electron dense lysosomes is that Al ingestions increased defective organelle turnover (e.g., mitophagy) and/or increased the reabsorption of extracellular matrix.

There is little evidence about the changes promoted by Al ingestion on the ultrastructure of osteoblasts using *in vivo* models. The mitochondrial alterations observed in this study corroborate

10.3389/fimag.2026.1725794

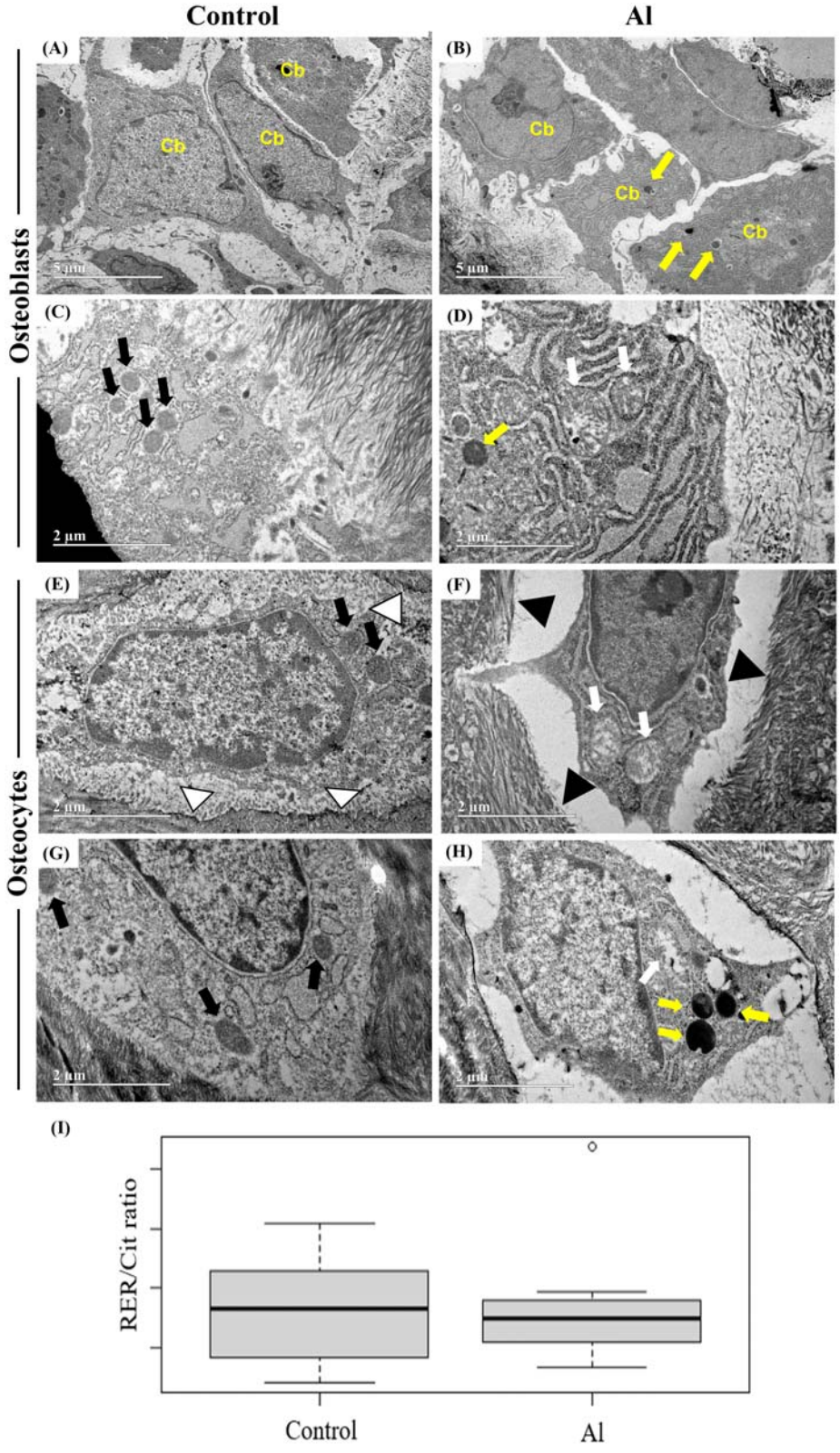

FIGURE 1
Osteoblasts and osteocytes ultrastructure. The microenvironment of osteoblasts is shown in the control **(A)** and Al **(B)** groups. The control group exhibited mitochondria with normal morphology and cristae in both osteoblasts **(C)** and osteocytes **(E, G)**. In the Al group, mitochondria showed swelling, distortions in the cristae **(D)** or disruption **(F, H)**. Ostecytes from the control group filled the lacuna completely and showed frequent osmiophilic layer **(E, G)**. Chondrocytes in the Al group showing retraction and rare osmiophilic layer **(F)**. I) Ratio between RER and cytoplasm in osteoblasts. The treatment with Al did not affect RER/Cit ratio ($p \geq 0.05$). Electron-dense lysosomes were more frequent in the Al group **(B, D, H)**. MET. Ob:osteoblasts; black arrow: normal mitochondria; white arrow: altered mitochondria; yellow arrow: eletron-dense lysossomes; white arrowhead: osmiophilic layer; black arrowhead: absence of osmiophilic layer.

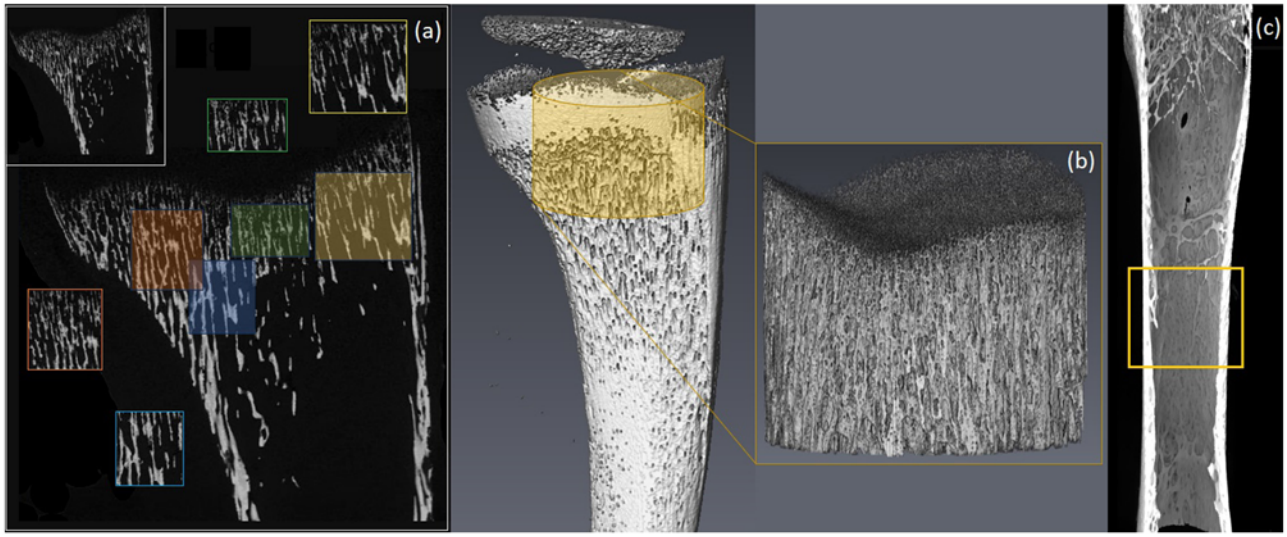

FIGURE 2
Process of VOI selection for trabecular **(a, b)** and cortical **(c)** bone. A cylinder (2 mm *d* x 2 mm *h*) VOI was chosen for trabecular analysis **(b)**. For cortical analysis, a 2 mm long VOI from the middle of the diaphysis was selected **(c)**.

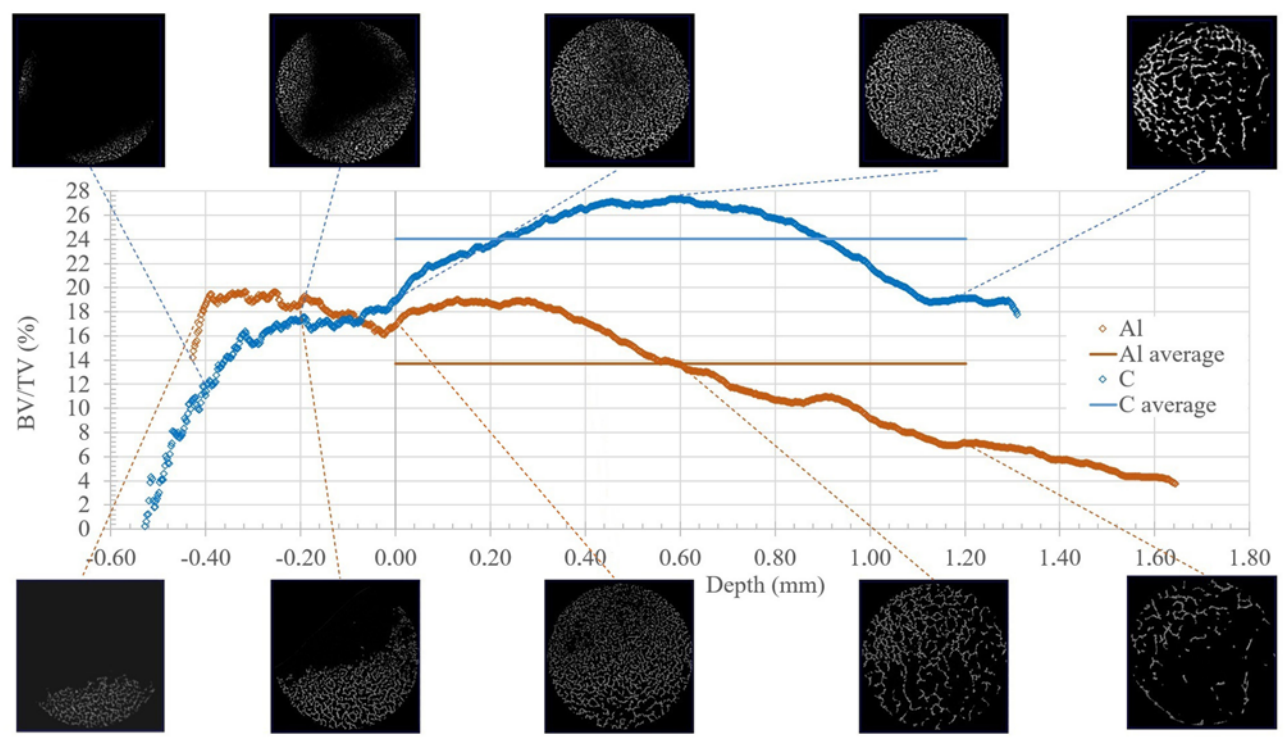

FIGURE 3
Distribution of 2D slices BV/TV throughout the analyzed VOI. Slices at negative depths correspond to the epiphyseal cartilage area. The initial region for trabecular bone analysis is represented as 0 mm. Lower BV/TV values are evident in the Al group with increasing VOI depth.

the results of ZHU and coworkers (Zhu et al., 2016) showing mitochondrial swelling, foam-like structure, and cytoplasmic spillover in rat osteoblasts after 120 days of AlCl3 feeding. Plachot et al. (1984) showed Al accumulation into the mitochondria and in the mineralization front of Al intoxicated hemodialyzed patients suffering from osteitis fibrosa, suggesting that Al impaired the mitochondria function and affected the mineralization process in those patients. Mitochondrial impairment has been associated to Aluminum in different tissues, such as neurons (Makhdoomi et al., 2023; Sharma et al., 2015) endometrium (Marwa et al., 2017), testis (Maghraoui et al., 2023), cardiomyocytes (Khezri et al., 2020), parathyroid gland (Cournot-Witmer and Plachot, 1990), and liver

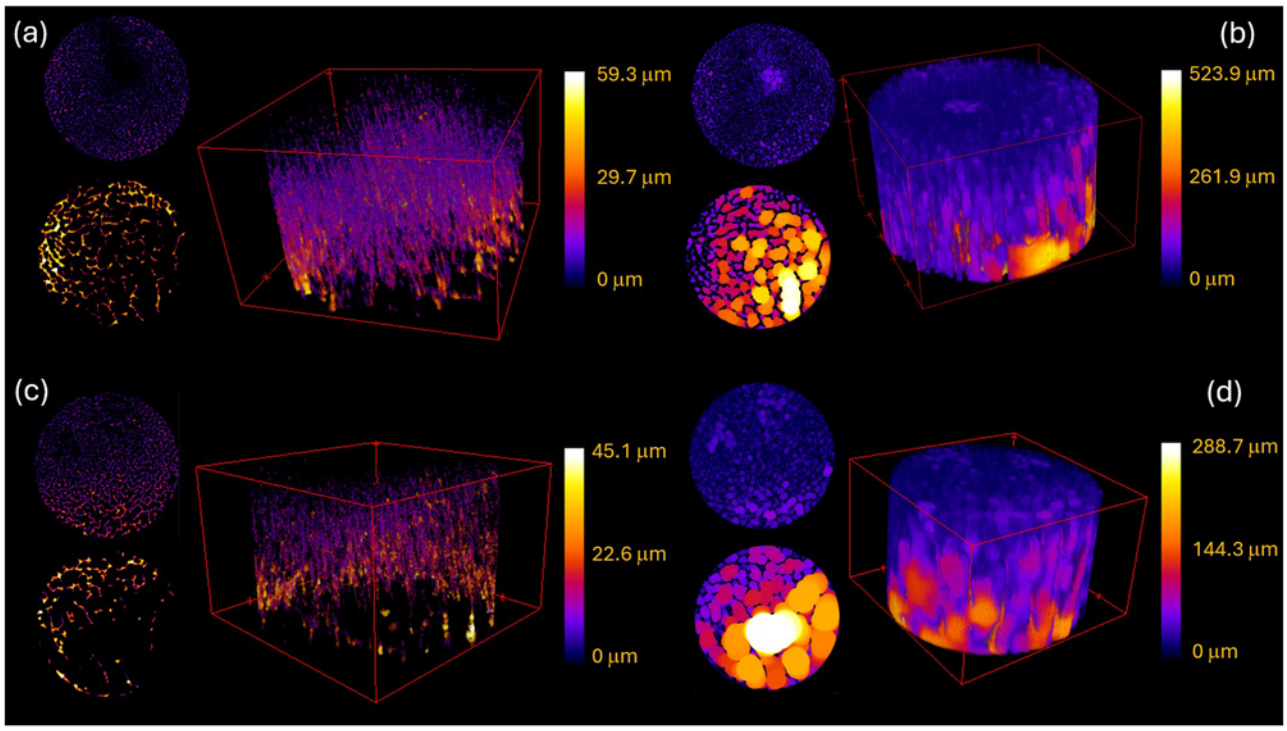

FIGURE 4
Tridimensional colormaps of Tb.Th and Tb.Sp for Control **(a, b)** and Al **(c, d)** groups, respectively. The scale bar employs a color gradient to illustrate the sizes ranging from dark blue (smaller size) to white (larger size).

TABLE 1 Micro-CT morphometric parameters in the tibia of newborn rats.

Parameter	Group	
	Control (C)	Aluminum (Al)
BV/TV (%)	24.1 ± 3.0	13.7 ± 4.0
Tb.Th (µm)	19.3 ± 8.5	16.5 ± 6.1
Tb.Sp (µm)	77.1 ± 55.8	148.3 ± 110
Tb.N (μm^{-1})	0.0104	0.0061
Ct.Th (µm)	197.1 ± 45.9	181.0 ± 42.9
Ct.np	116.0 ± 11.7	118.2 ± 6.6
Co.Po (%)	11.7 ± 1.6	12.4 ± 1.5

BV/TV, Bone Volume/Tissue Volume; Tb.th, trabecular thickness; Tb.Sp, trabecular spacing; Tb.N, trabecular number; Ct.Th, cortical thickness; Ct.np, cortical pores number; Co.Po, cortical porosity; Conn.D, connectivity density.

(Xu et al., 2017); recently, CUI and coworkers (Cui et al., 2021) showed mitophagy induced by aluminum in rat femora.

Studies *in vitro* show similar results in osteoblasts (Florent et al., 1991), fibroblasts (Xu et al., 2017), neurons (Makhdoomi et al., 2023) and endometrium (da Silva Lima et al., 2020) highlighting mitochondrial distortion, foamy appearance of the cytoplasm, uneven chromatin distribution, defects in the cytoplasmic membrane and cell swelling. Mitochondria is an important site for the production and elimination of reactive oxygen species (ROS) in cells, and dysfunctional mitochondria favors the negative effect of ROS on osteogenesis reducing osteoblastic activity and altering bone architecture (Zhang et al., 2023; Kimball et al., 2021).

Osteocytes are embedded in a mineralized matrix and its role in orchestrating bone remodeling by coordinating osteoblasts and osteoclasts activity is well described (Siddiqui and Partridge, 2016; Zhu et al., 2022; Anloague and Delgado-Calle, 2023). Additionally, osteocytes are able to directly regulate their own microenvironment by remodeling the peri lacunar matrix in physiological and pathological situations in a process known as osteocytic osteolysis (Tsourdi et al., 2018; Moreno-Jiménez et al., 2024), recognized by specific morphological characteristics. In the Al group the osteocytes had the classical characteristics of resorptive osteocytes as abundant RER, increased lysosomes and absent osmiophilic layer in the lacunae (Bélanger, 1969; Ross and Pawlina, 2021). Osteocytic osteolysis increases in pathological conditions, such as hyperparathyroidism, bone metastasis and osteoporosis (Anloague and Delgado-Calle, 2023). Based on the TEM analysis, it was demonstrated that Al brought about considerable changes regarding osteocytic osteolysis in the osteocytes, thus implicating these cells in bone matrix degradation.

Osteocytes are the primary regulators of bone remodeling in response to mechanical forces, playing a central role in the maintenance of bone homeostasis and in the modulation of key cellular functions. This regulation occurs through peri-lacunar remodeling (PLR), a process by which osteocytes deposit and resorb extracellular matrix, as well as through their interactions with matrix constituents and cell–cell communication within the lacuno-canalicular system (Dole et al., 2017; Qin et al., 2021). In the present study, Al induced pronounced osteocyte retraction,

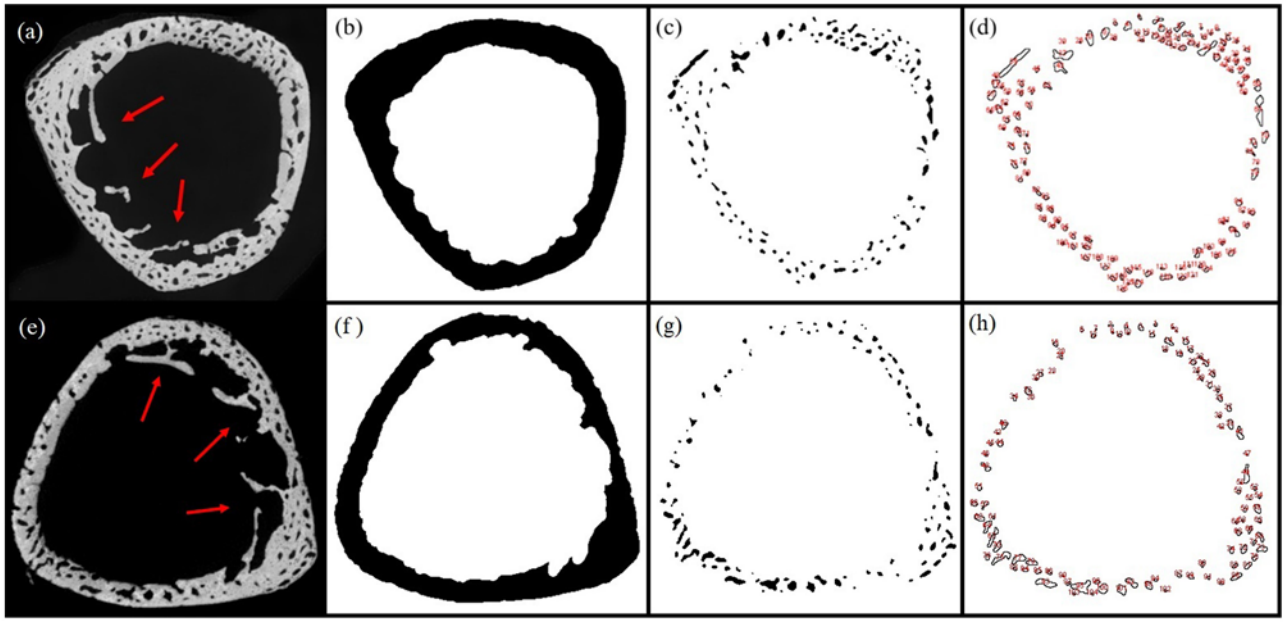

FIGURE 5
Original 2D slices from Control **(a)** and Al **(e)** groups; red arrows indicate trabecular formations. Resulting binary images following image processing **(b, f)** show the removal of pores and trabeculae. Isolated pores **(c, g)** were subsequently quantified **(d, h)**.

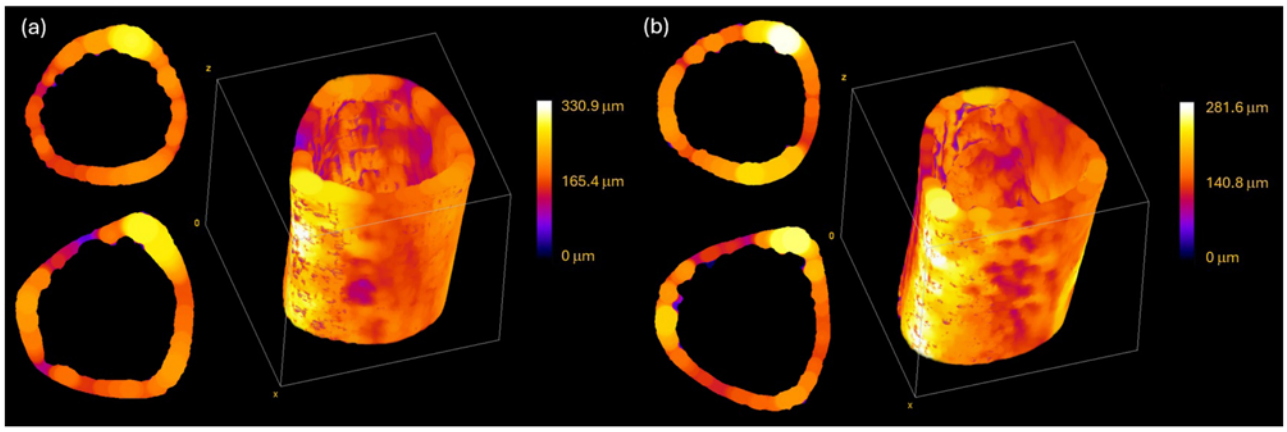

FIGURE 6
Tridimensional colormaps of Ct.Th for Control **(a)** and Al **(b)** groups, respectively. Cortical bone was thicker in the anterior margin of the tibia in both Control and Al group (whitish color). The first and last corresponding 2D slices are positioned alongside the VOI.

which may compromise both osteocyte–matrix interactions in the peri-lacunar space and the connectivity among cytoplasmic processes within the lacuno-canalicular network, thereby impairing mechanically driven bone remodeling (Qin et al., 2020). Our findings did not demonstrate the presence of Al within the bone matrix, which limits conclusions regarding whether matrix-associated Al directly affects cellular interactions. Integrins are known to play a critical role in cell–matrix interactions, and the β3 integrin subunit has been directly implicated in bone mass accrual (Qin et al., 2023). Therefore, investigating the effects of Al on the lacuno-canalicular system (LCS), integrin expression, and the integrity of focal adhesions between osteocytes may represent an important step toward elucidating the mechanisms by which Al disrupts bone metabolism.

Our results showed that osteoblasts and osteocytes remained active but exhibited considerable lysosomal accumulation and altered mitochondrial structure in aluminum-treated animals. In general, the dynamics of mitochondria are reflected in their function and morphology (Qin et al., 2021; Chen et al., 2016) and the remodeling of their cristae influences the protein complexes of the respiratory chain (Cogliati et al., 2016, 2013) impacting the efficiency of oxidative phosphorylation and cell function (Dougherty and Kunzelmann, 2007; Doube et al., 2010; Chan, 2020). The biomechanical performance of the trabecular bone is influenced by its mass and especially its macroarchitecture (Hom and Sheu, 2009). The ultrastructural alterations observed in the Al group probably influenced the quality and the amount of bone matrix, compromising bone architecture. In addition to a reduction

in important matrix proteins such as Osteocalcin and Collagen, a previous study of our group demonstrated a considerable reduction on bone morphometric parameters as Bone Matrix (%), trabecular number (Tb.N), trabecular width (Tb.wi) and cortical width (Ct.wi), (Marques et al., 2022). In the present study, the micro-CT analysis provided complementary data showing that these bone parameters reduced throughout the analyzed VOI. In addition to generating quantitative data, the micro-CT technique provides a more complete visual overview of the specimens, allowing the results to be projected more reliably onto the entire tissue and highlighting the importance of selecting a proper VOI for analysis.

The morphometric parameters commonly determined by image analysis software and presented in scientific papers are typically based on 2D squared images or cuboid VOIs. Figure 2 shows that these determinations can be misleading if the object of analysis is restricted to a squared or a cuboid image. Another highlight of the micro-CT technique is its ability to show how a parameter varies throughout the specimen, and not just to determine its value. As seen in Figure 3, the BV/TV values for both groups are quite different overall, yet they converge at the same value for a specific depth (17.2% at −0.08 mm).

Results from the micro-CT analyses demonstrated that Al negatively affected the cortical and the cancellous microarchitecture reducing BV/TV, Ct.Th, Tb.Th, Tb.N and increasing Tb.Sp. Our results are consistent with the literature that demonstrates the toxic effect of Al on bone, such as reduction of Tb.th and Ct.th in addition to bone mineral content (BMC) (Liang et al., 2018; Chen et al., 2016).

Bone formation was reduced in the treated group, even though active osteoblasts indicated that Al played an attenuation role on these cells and decreased bone matrix deposition, reflecting on thinner trabeculae. Such a pattern of loss has a benign prognosis because the thinning trabeculae can be thickened, yet the replacement of lost trabeculae is a complex process (Liang et al., 2018; An and Martin, 2003). In this sense, it would be interesting to evaluate the long-term effects of Al on bone microarchitecture after neonatal exposure in addition to evaluating the self-recovery capacity of the tissue. Hence, this would be an important predictor of the real effects of the diary Al doses ingested by the population. Another interesting approach could be to propose alternatives to prevent bone changes caused by aluminum intake using, for example, exogenous antioxidants, which have shown positive effects on bone formation (Kimball et al., 2021; Dougherty and Kunzelmann, 2007).

5 Conclusion

This study showed that aluminum feeding during the neonatal phase affects osteoblast and osteocyte ultrastructure, suggesting that it may affect bone formation. In addition to warning about the need to control the amount of Al ingested, it is important to investigate efficient ways to reverse the effects of Al on bone tissue, especially in the most susceptible groups, such as newborns.

Data availability statement

The raw data supporting the conclusions of this article will be made available by the authors, without undue reservation.

Ethics statement

The animal study was approved by Animal Use Ethics Committee (CEUA/UFG protocol no. 100/19). The study was conducted in accordance with the local legislation and institutional requirements.

Author contributions

MM: Conceptualization, Project administration, Writing – original draft, Writing – review & editing. AM: Formal analysis, Resources, Writing – original draft. IM: Investigation, Validation, Writing – review & editing. PB: Investigation, Resources, Writing – review & editing. IN: Investigation, Visualization, Writing – review & editing. CF: Resources, Supervision, Writing – review & editing. FS: Resources, Supervision, Writing – review & editing.

Funding

The author(s) declared that financial support was not received for this work and/or its publication.

Acknowledgments

The authors thank Dra. Tatiane Oliveira dos Santos and the Multiuser Laboratory of High-Resolution Microscopy at the Federal University of Goiás for the kind support with the transmission electron microscopy and the Laboratory of Porous Media and Thermophysical Properties (LMPT) for the micro-CT analysis.

Conflict of interest

The author(s) declared that this work was conducted in the absence of any commercial or financial relationships that could be construed as a potential conflict of interest.

The author(s) AM and IM declared that they were an editorial board member of Frontiers, at the time of submission. This had no impact on the peer review process and the final decision.

Generative AI statement

The author(s) declared that generative AI was not used in the creation of this manuscript.

Any alternative text (alt text) provided alongside figures in this article has been generated by Frontiers with the support of artificial intelligence and reasonable efforts have been made to ensure accuracy, including review by the authors wherever possible. If you identify any issues, please contact us.

Publisher's note

References

An, Y. H., and Martin, K. L. (2003). *Handbook of histology methods for bone and cartilage, 1st ed*. Totowa, NJ: Humana Press. doi: 10.1385/1592594174

Anloague, A., and Delgado-Calle, J. (2023). Osteocytes: new kids on the block for cancer in bone therapy. *Cancers* 15:2645. doi: 10.3390/cancers15092645

Bélanger, L. F. (1969). Osteocytic osteolysis. *Calcif Tissue Res.* 4, 1–12. doi: 10.1007/BF02279101

Bougle, D., Bureau, F., Voirin, J., and Duhamel, J. F. (1991). [Aluminum level in infants. Comparison between full-term and premature newborn infants]. *Arch Fr Pediatr.* 48, 299–300.

Chan, D. C. (2020). Mitochondrial dynamics and its involvement in disease. *Ann. Rev. Pathol.* 15, 235–259. doi: 10.1146/annurev-pathmechdis-012419-032711

Chen, C., Jin, D., Liu, Y., Wehrli, F. W., Chang, G., Snyder, P. J., et al. (2016). Trabecular bone characterization on the continuum of plates and rods using *in vivo* MR imaging and volumetric topological analysis. *Phys Med Biol.* 61, N478–496. doi: 10.1088/0031-9155/61/18/N478

Chen, X., Zhang, A., Zhao, K., Gao, H., Shi, P., Chen, Y., et al. (2024). The role of oxidative stress in intervertebral disc degeneration: mechanisms and therapeutic implications. *Ageing Res Rev.* 98:102323. doi: 10.1016/j.arr.2024.102323

Cogliati, S., Enriquez, J. A., and Scorrano, L. (2016). Mitochondrial cristae: where beauty meets functionality. *Trends Biochem. Sci.* 41, 261–73. doi: 10.1016/j.tibs.2016.01.001

Cogliati, S., Frezza, C., Soriano, M. E., Varanita, T., Quintana-Cabrera, R., Corrado, M., et al. (2013). Mitochondrial cristae shape determines respiratory chain supercomplexes assembly and respiratory efficiency. *Cell.* (2013) 155, 160–171. doi: 10.1016/j.cell.2013.08.032

Cournot-Witmer, G., Gagnadoux, M. F., Lebon, P., Broyer, M., and Balsan, S. (1982). [Osteomalacia as a result of aluminum poisoning during chronic hemodialysis]. *Arch. Fr. Pediatr.* 2, 749–54.

Cournot-Witmer, G., and Plachot, J. J. (1990). Parathyroid glands in chronic aluminum intoxication. *Ultrastruct. Pathol.* 14, 211–219. doi: 10.3109/01913129009076125

Cui, Y., Song, M., Xiao, B., Liu, M., Liu, P., Han, Y., et al. (2021). ROS-mediated mitophagy and apoptosis are involved in aluminum-induced femoral impairment in mice. *Chem. Biol. Interact.* 349:109663. doi: 10.1016/j.cbi.2021.109663

da Silva Lima, D., da Silva Gomes, L., de Sousa Figueredo, E., de Godoi, M. M., Silva, E. M., Silva Neri, H. F., et al. (2020). Aluminum exposure promotes histopathological and pro-oxidant damage to the prostate and gonads of male and female adult gerbils. *Exp Mol Pathol.* 116:104486. doi: 10.1016/j.yexmp.2020.104486

Dole, N. S., Mazur, C. M., Acevedo, C., Lopez, J. P., Monteiro, D. A., Fowler, T. W., et al. (2017). Osteocyte-intrinsic TGF-β signaling regulates bone quality through perilacunar/canalicular remodeling. *Cell Rep.* 21, 2585–2596. doi: 10.1016/j.celrep.2017.10.115

Doube, M., Kłosowski, M. M., Arganda-Carreras, I., Cordelières, F. P., Dougherty, R. P., Jackson, J. S., et al. (2010). BoneJ: free and extensible bone image analysis in ImageJ. *Bone* 47, 1076–1079. doi: 10.1016/j.bone.2010.08.023

Dougherty, R., and Kunzelmann, K. (2007). Computing local thickness of 3D structures with ImageJ. *Microsc. Microanal.* 13, 1678–1679. doi: 10.1017/S1431927607074430

Exley, C. (2016). The toxicity of aluminium in humans. *Morphologie* 100, 51–5. doi: 10.1016/j.morpho.2015.12.003

Florent, C., Desaint, B., Legendre, C., Chappuis, P., Galle, C., Giboudeau, J., et al. (1991). Morphologic and ultrastructural effects of maalox tc on human gastric and duodenal mucosa. *J. Clin. Gastroenterol.* 13, S139–44. doi: 10.1097/00004836-199112001-00023

Hadrup, N., Sørli, J. B., Jenssen, B. M., Vogel, U., and Sharma, A. K. (2024). Toxicity and biokinetics following pulmonary exposure to aluminium (aluminum): A review. *Toxicology* 506:153874. doi: 10.1016/j.tox.2024.153874

Hartung, N., Wangorsch, G., Huisinga, W., and Weisser, K. (2025). Extension and validation of a physiologically based toxicokinetic model for risk assessment of aluminium exposure in humans. *Arch Toxicol.* 99, 2379–2395. doi: 10.1007/s00204-025-04031-1

Hewitt, C. D., Savory, J., and Wills, M. R. (1990). Aspects of aluminum toxicity. *Clin. Lab. Med.* 10, 403–422. doi: 10.1016/S0272-2712(18)30576-6

Hom, J., and Sheu, S. S. (2009). Morphological dynamics of mitochondria–a special emphasis on cardiac muscle cells. *J. Mol. Cell Cardiol.* 46, 811–820. doi: 10.1016/j.yjmcc.2009.02.023

Khezri, S., Sabzalipour, T., Jahedsani, A., Azizian, S., Atashbar, S., Salimi, A., et al. (2020). Chrysin ameliorates aluminum phosphide-induced oxidative stress and mitochondrial damages in rat cardiomyocytes and isolated mitochondria. *Environ. Toxicol.* 35, 1114–1124. doi: 10.1002/tox.22947

Kimball, J. S., Johnson, J. P., and Carlson, D. A. (2021). Oxidative stress and osteoporosis. *J. Bone Joint Surg. Am.* 103, 1451–1461. doi: 10.2106/JBJS.20.00989

Klein, G. L. (2019). Aluminum toxicity to bone: A multisystem effect? *Osteoporos Sarcopenia* 5, 2–5. doi: 10.1016/j.afos.2019.01.001

Liang, H., Gao, J., Zhang, C., Li, C., Wang, Q., Fan, J., et al. (2018). Nicotinamide mononucleotide alleviates aluminum induced bone loss by inhibiting the TXNIP-NLRP3 inflammasome. *Toxicol. Appl. Pharmacol.* 362, 20–7. doi: 10.1016/j.taap.2018.10.006

Lindblad, E. B. (2004). Aluminium adjuvants - In retrospect and prospect. *Vaccine* 22, 3658–3568. doi: 10.1016/j.vaccine.2004.03.032

Maghraoui, S., Florea, A., Ayadi, A., Matei, H., and Tekaya, L. (2023). Changes in organ weight, sperm quality and testosterone levels after aluminum (Al) and Indium (In) administration to wistar rats. *Biol. Trace Elem. Res.* 201, 766–775. doi: 10.1007/s12011-022-03180-z

Makhdoomi, S., Ariafar, S., Mirzaei, F., and Mohammadi, M. (2023). Aluminum neurotoxicity and autophagy: a mechanistic view. *Neurol Res.* 45, 216–225. doi: 10.1080/01616412.2022.2132727

Malluche, H. H., and Faugere, M. C. (1988). Aluminum-related bone disease. *Blood Purif.* 6, 1–15. doi: 10.1159/000169479

Marques, M. R., de Assis, P. H. G., Azeredo, P. S., Fleury, J. A., Costa, J. R., Gomes, L. S., et al. (2022). Aluminum intake in the neonatal phase disrupts endochondral ossification in rodents. *J. Trace Elem. Med. Biol.* 72:126962. doi: 10.1016/j.jtemb.2022.126962

Marwa, M., Adrian, F., Nedra, B., Samira, M., Horea, M., Walid-Habib, T., et al. (2017). The role of lysosomes in the phenomenon of concentration of aluminum and indium in the female reproductive system. An ultrastructural study. *J. Trace Elem. Med. Biol.* 44, 59–64. doi: 10.1016/j.jtemb.2017.05.009

Moreno-Jiménez, I., Heinig, S., Heras, U., Maichl, D. S., Strifler, S., Leich, E., et al. (2024). 3D osteocyte lacunar morphometry of human bone biopsies with high resolution microCT: From monoclonal gammopathy to newly diagnosed multiple myeloma. *Bone* 1:189. doi: 10.1016/j.bone.2024.117236

Plachot, J. J., Cournot-Witmer, G., Halpern, S., Mendes, V., Bourdeau, A., Fritsch, J., et al. (1984). Bone ultrastructure and x-ray microanalysis of aluminum-intoxicated hemodialyzed patients. *Kidney Int.* 25, 796–803. doi: 10.1038/ki.1984.92

Qin, L., Chen, Z., Yang, D., He, T., Xu, Z., Zhang, P., et al. (2023). Osteocyte β3 integrin promotes bone mass accrual and force-induced bone formation in mice. *J. Orthop. Translat.* 40, 58–71. doi: 10.1016/j.jot.2023.05.001

Qin, L., Fu, X., Ma, J., Lin, M., Zhang, P., Wang, Y., et al. (2021). Kindlin-2 mediates mechanotransduction in bone by regulating expression of Sclerostin in osteocytes. *Commun Biol.* 4:402. doi: 10.1038/s42003-021-01950-4

Qin, L., Liu, W., Cao, H., and Xiao, G. (2020). Molecular mechanosensors in osteocytes. *Bone Res.* 8:23. doi: 10.1038/s41413-020-0099-y

Ross, M. H., and Pawlina, W. (2021). *Ross Histología - Texto y Atlas. 8th ed.* Mendoza C, Llavina N, editors. Barcelona: Wolters Kluer p. 241–242.

Sharma, D. R., Sunkaria, A., Wani, W. Y., Sharma, R. K., Verma, D., Priyanka, K., et al. (2015). Quercetin protects against aluminium induced oxidative stress and promotes mitochondrial biogenesis via activation of the PGC-1α signaling pathway. *Neurotoxicology* 51, 116–137. doi: 10.1016/j.neuro.2015.10.002

Siddiqui, J. A., and Partridge, N. C. (2016). Physiological bone remodeling: systemic regulation and growth factor involvement. *Physiology* 31, 233–45. doi: 10.1152/physiol.00061.2014

Tsourdi, E., Jähn, K., Rauner, M., Busse, B., and Bonewald, L. F. (2018). Physiological and pathological osteocytic osteolysis. *J. Musculoskelet. Neuronal Interact.* 18, 292–303

Xu, F., Liu, Y., Zhao, H., Yu, K., Song, M., Zhu, Y., et al. (2017). Aluminum chloride caused liver dysfunction and mitochondrial energy metabolism disorder in rat. *J. Inorg. Biochem.* 174, 55–62. doi: 10.1016/j.jinorgbio.2017.04.016

Yokel, R. A. (2020). Aluminum reproductive toxicity: a summary and interpretation of scientific reports. *Crit. Rev. Toxicol.* 50, 551–93. doi: 10.1080/10408444.2020.1801575

Yokel, R. A. (2025). Aluminum in beverages and foods: A comprehensive compilation of regulations; concentrations in raw, prepared, and stored beverages and foods; and intake. *Compr. Rev. Food Sci.* 24:70175. doi: 10.1111/1541-4337.70175

Zhang, C., Li, H., Li, J., Hu, J., Yang, K., Tao, L., et al. (2023). Oxidative stress: a common pathological state in a high-risk population for osteoporosis. *Biomed. Pharm.* 163:114834. doi: 10.1016/j.biopha.2023.114834

Zhu, C., Shen, S., Zhang, S., Huang, M., Zhang, L., Chen, X., et al. (2022). Autophagy in bone remodeling: a regulator of oxidative stress. *Front. Endocrinol.* 30:13. doi: 10.3389/fendo.2022.898634

Zhu, Y., Xu, F., Yan, X., Miao, L., Li, H., Hu, C., et al. (2016). The suppressive effects of aluminum chloride on the osteoblasts function. *Environ. Toxicol. Pharmacol.* 48, 125–129. doi: 10.1016/j.etap.2016.10.009